

Reconstructing the gravitational field of the local universe

Harry Desmond^{1,2*}, Pedro G. Ferreira³, Guilhem Lavaux^{4,5} and
Jens Jasche⁶

¹*Kavli Institute for Particle Astrophysics and Cosmology, Physics Department, Stanford University, Stanford, CA 94305, USA*

²*SLAC National Accelerator Laboratory, Menlo Park, CA 94025, USA*

³*Astrophysics, University of Oxford, DWB, Keble Road, Oxford OX1 3RH, UK*

⁴*Sorbonne Universités, UPMC Univ Paris 6 et CNRS, UMR 7095, Institut d’Astrophysique de Paris, 98 bis bd Arago, 75014 Paris, France*

⁵*Sorbonne Universités, Institut Lagrange de Paris (ILP), 98 bis bd Arago, 75014 Paris, France*

⁶*Excellence Cluster Universe, Technische Universität München, Boltzmannstrasse 2, D-85748 Garching, Germany*

21 July 2022

ABSTRACT

Tests of gravity at the galaxy scale are in their infancy. As a first step to systematically uncovering the gravitational significance of galaxies, we map three fundamental gravitational variables – the Newtonian potential, acceleration and curvature – over the galaxy environments of the local universe to a distance of approximately 200 Mpc. Our method combines the contributions from galaxies in an all-sky redshift survey, halos from an N-body simulation hosting low-luminosity objects, and linear and quasi-linear modes of the density field. We use the ranges of these variables to determine the extent to which galaxies expand the scope of generic tests of gravity and are capable of constraining specific classes of model for which they have special significance. Finally, we investigate the improvements afforded by upcoming galaxy surveys.

Key words: gravitation – galaxies: fundamental parameters – galaxies: kinematics and dynamics – galaxies: statistics

1 INTRODUCTION

General Relativity (GR) has been the reigning paradigm of gravity for almost a century, and yet there is no shortage of alternatives. A range of possible reasons to extend or replace GR has been explored in the literature, including the attempt to overcome theoretical or conceptual difficulties, obviate the need for dark energy or alleviate the cosmological constant problem, account more precisely for astrophysical phenomena, or simply investigate the range of gravity theories consonant with basic physical principles or that may have interesting observational consequences (see e.g. Clifton et al. 2012 and references therein). These diverse motivations have led to a large and heterogeneous parameter space of models which cannot be thoroughly probed by traditional tests. Instead, systematic progress will require the synthesis of evidence from across the range of scales accessible to observation and experiment.

To date, most effort has been devoted to probing gravity in three types of system: the laboratory, the Solar System, and the linear and quasi-linear cosmological regimes. In the laboratory, tests of the equivalence principle (EP) on which GR is premised have now reached $\mathcal{O}(10^{-13})$ precision (Schlamminger et al. 2008), severely limiting de-

viations from the inverse square law. Within the Solar System, the Parameterised Post-Newtonian (PPN) framework has enabled the coefficients of general metric theories to be constrained at leading relativistic order, providing tight limits on the coupling of extra fields to matter and generic deviations from standard weak-field equations of motion (Nordtvedt 1968; Will 1993). In cosmology, GR is combined with the hypotheses of dark matter and dark energy to form the Λ CDM model, which may be probed via its predictions for Big Bang Nucleosynthesis, the Cosmic Microwave Background, the expansion history of the universe and the growth rate of structure (e.g. Bull et al. 2016 and references therein). Analogously to PPN, frameworks have also been devised to test generic deviations from standard cosmological metrics (e.g. Baker et al. 2013). In none of these cases has a convincing deviation from GR been found.

Nevertheless, these tests do not cover the full range of systems in which deviations from GR may appear, and modified gravity theories may be constructed which satisfy all current experimental bounds and yet exhibit divergent behaviour elsewhere. The possibility that GR may break in some systems – or as a function of certain variables – but not others decouples tests in different regimes, and introduces the possibility that novel gravitational signals may be sequestered in regions of parameter space so far unexplored. Indeed, the notion that physical theories break down at crit-

* E-mail: harryd2@stanford.edu

ical values of certain variables, and hence in select systems, is not new: Galilean Relativity gives way to Special at v near c , and Newtonian gravity to GR at Φ near c^2 . Other variables, in which present tests span only a limited range of values, may mark the onset of new gravitational regimes.

The aim of this paper is to contribute to the development of tests of GR in a qualitatively different and relatively under-explored regime: the galactic. In particular, we see the galaxy scale as able to extend the scope of gravitational probes in three main ways:

(i) Many scalar-tensor theories of gravity must employ a “screening mechanism” to suppress their fifth force in the Solar System and laboratory. This may be achieved either by the scalar field acquiring a high mass and hence short range when large (chameleon screening; [Khouri & Weltman 2004](#)), or by kinetic (kinetic screening; [Babichev et al. 2009](#)) or higher order (Vainshtein screening; [Vainshtein 1972](#)) terms in the Lagrangian becoming dominant. In each case the degree of screening is governed by a different function of the scalar field, which simulations have shown to correlate with simple Newtonian proxies: the potential Φ for chameleon screening, acceleration \vec{a} for kinetic, and some function of the Riemann tensor – we will call it the “curvature” K – for Vainshtein ([Cabr e et al. 2012](#); [Khouri 2013](#)). For typical scalar-tensor theories, the transitions between screened and unscreened regions occur at values of these proxies characteristic of galaxies and their environments ([Hui et al. 2009](#); [Jain & VanderPlas 2011](#)); GR is recovered at the larger values that describe laboratory and Solar System tests. Further, for a broad class of chameleon-like theories laboratory fifth force constraints imply a range for the scalar field at cosmological densities of $\lesssim 1$ Mpc, rendering its impact on linear perturbations and the universe’s expansion history negligible ([Wang et al. 2012](#)). This makes the intermediate galaxy scale the ideal one at which to test such models.

(ii) A dependence of the kinematics of any system on the external gravitational field constitutes a violation of the equivalence principle (EP), and *a fortiori* of GR. The EP has been tested precisely in the lab (at $a \approx 10 \text{ ms}^{-2}$) and inner Solar System ($a \approx 10^{-2} \text{ ms}^{-2}$). Galaxies, however, have characteristic accelerations at least six orders of magnitude lower, and hence allow for EP tests in a very different region of parameter space. Beside the case of screening described above (in which EP violation is typically effective at the macroscopic level, rather than fundamental at the level of the action), a paradigmatic example of a theory that exploits this gap to violate the EP is Modified Newtonian Dynamics (MOND; [Milgrom 1983a,b,c](#)). This phenomenon is known in MOND as the “external field effect,” whereby a large external acceleration can render a system’s dynamics Newtonian or quasi-Newtonian even for internal accelerations much below the threshold value $a_0 \approx 10^{-10} \text{ ms}^{-2}$. As explained further in Section 4.1, galaxies’ mass-to-light ratios and the shapes of their rotation and velocity dispersion profiles would be expected to correlate with external field strength when the latter was sufficiently high, enabling the theory to be tested by means of a prediction complementary to the more conventional ones concerning the internal field alone. Indeed, galaxy environments are among the only with accelerations at and around a_0 , and hence are uniquely capable of testing this and related models.

(iii) [Baker et al. \(2015\)](#) mapped out the theoretical and experimental gravity parameter space in terms of Φ and K , and discovered that the curvature values of galaxies are not currently probed by any observational test. These values separate the relatively well-studied small-scale regime at high K from the ‘troubled’ cosmological regime at low K , leading [Baker et al. \(2015\)](#) to suggest they may be a natural place for novel gravitational physics to emerge. Since galaxies are the *only* systems to inhabit this region of parameter space, they are the only ones *in principle* capable of probing it, regardless of measurement precision.

These motivations suggest we focus on three gravitational variables at the galaxy scale: the Newtonian potential Φ , acceleration \vec{a} and curvature K . More generally, these are among the most basic descriptors of the gravitational field, and may therefore be expected *a priori* to characterise the transitions between gravitational regimes. In the weak-field limit for a set of point masses (as describes galaxies), they scale as M/r , M/r^2 and M/r^3 respectively, and hence provide a range of relative scalings with the variables M and r that determine an object’s gravitational influence.

The first step towards identifying novel gravitational physics associated with one or more of these variables is to map out their values over the local universe. That is the task of this paper. In particular, we will build maps of Φ , \vec{a} and K out to ~ 200 Mpc by combining the contributions of galaxies measured in an all-sky survey, halos in an N-body simulation hosting galaxies too faint to be observed, and long-wavelength density modes not captured by the halo population. Given a set of galaxies with measurements for potential modified gravity signals, these maps will allow the signals’ correlations with each gravitational variable to be determined, and hence the theories above to be investigated and gaps in the experimental parameter space filled in. This will be the subject of future work.

The only previous work along these lines is [Cabr e et al. \(2012\)](#), who focus on Φ as an estimator of the degree of screening in chameleon theories. Besides extending to \vec{a} and K , our analysis will build on this pioneering study in several ways: we will use a more complete and homogeneous all-sky source catalogue, apply more sophisticated methods for determining source objects’ mass distributions from their magnitudes, and calibrate and supplement the basic maps with N-body simulations and estimates of the quasi-linear density field respectively. Unlike [Cabr e et al. \(2012\)](#), we will make no attempt to relate our proxies to features of specific theories through modified gravity simulations, but focus instead on mapping the gravitational variables most robustly. This will allow our results to retain full generality for future application to any model in which these variables are significant. Further comparison between our work and that of [Cabr e et al. \(2012\)](#) is given in Section 4.1.

The structure of this paper is as follows. In Section 2 we describe our method for constructing maps of Φ , \vec{a} and K , and in Section 3 we present the results. Section 4 applies our findings to modified gravity, describes the main sources of uncertainty, and discusses the improvements in precision achievable by upcoming galaxy surveys. Section 5 concludes.

2 METHOD

We make two general methodological comments before detailing our 3-step procedure.

While each of Φ , \vec{a} and K has an “internal” and “external” component, the first due to an object’s own mass and the second that of its environment, we will focus solely on the environmental contribution, which is a function purely of spatial position. The internal component depends on objects’ masses, and must therefore be calculated specifically for a given test galaxy sample. As Φ , \vec{a} and K are our estimators for the degrees of freedom in which GR may receive corrections, we refer to them hereafter as “proxies.”

The Newtonian potential Φ diverges when calculated in a sphere of $r \rightarrow \infty$, making it necessary to impose a cutoff distance r_{\max} . Chameleon-screened theories that motivate our investigation of Φ supply a natural choice for r_{\max} , the Compton wavelength λ_C of the scalar field that determines the effective range of the fifth force. Masses significantly further apart than λ_C interact little via the scalar coupling even if the field is otherwise unscreened. In $f(R)$ gravity, λ_C is set by the background field value f_{R0} , which also determines the potential Φ_{crit} at which screening becomes operative (Hu & Sawicki 2007; Cabré et al. 2012):

$$\lambda_C \approx 32 \sqrt{f_{R0}/10^4} \text{ Mpc}, \quad (1)$$

$$\Phi_{\text{crit}}/c^2 \approx \frac{3}{2} f_{R0}. \quad (2)$$

The f_{R0} scale that may be probed by galaxies is therefore set by typical values of Φ , which is a function of r_{\max} . We will see in Section 3.3 that Φ/c^2 is typically $\sim 10^{-5}$ for $r_{\max} = 10$ Mpc, which satisfies Eq. 1 for $r_{\max} = \lambda_C$. Φ decreases by only a few tenths of a dex for $r_{\max} = 3$ Mpc, which corresponds to $\Phi_{\text{crit}}/c^2 = 10^{-6}$. We will therefore adopt a fiducial value $r_{\max} = 10$ Mpc, although we will show results for $r_{\max} = 3$ Mpc also. Since our other proxies (\vec{a} and K) fall off more steeply with r (and individual contributions to \vec{a} sum vectorially), sources beyond 3 Mpc typically contribute little, making them fairly insensitive to the choice of r_{\max} . Their values are normally set by a few nearby objects.

2.1 Primary source catalogue

We base our analysis on the 2M++ galaxy catalogue (Lavaux & Hudson 2011), a synthesis of 2MASS, 6dF and SDSS data. This is an optimum catalogue for our purposes, for three reasons. First, it was designed with the goal of high all-sky completeness out to 200 Mpc. Complete sky coverage will prevent our having to restrict our maps to the footprint of a single survey, and 200 Mpc is around the largest distance that potential modified gravity signals are robustly measurable at present (Vikram et al. 2013). Deeper surveys (e.g. the SDSS main sample) exist only over part of the sky. Second, it has a homogeneous limiting K -band magnitude ($m_K < 12.5$), which will facilitate our modelling of the contributions to the proxies from missing objects by means of an N-body simulation in Section 2.2. Finally, the catalogue has already been used to estimate the linear and quasi-linear modes of the density field in the survey volume (Lavaux & Jasche 2016), which provide important con-

tributions to our proxies yet cannot be reconstructed from the halo model applied to an N-body simulation.

To determine the values of Φ , \vec{a} and K sourced by the 2M++ galaxies, we first estimate the mass distributions of their dark matter halos. We utilise the technique of “halo abundance matching,” which maps galaxies to halos produced in an N-body simulation by postulating a nearly monotonic relationship between luminosity and some function of halo virial mass and concentration (Kravtsov et al. 2004; Conroy et al. 2006; Moster et al. 2010). For a suitable scatter and function of halo properties, this has been shown to yield excellent agreement with galaxy clustering statistics (e.g. Reddick et al. 2013; Lehmann et al. 2015) and moderate agreement with galaxies’ internal dynamics (e.g. Trujillo-Gomez et al. 2011; Desmond & Wechsler 2015, 2016; Desmond 2017). We use the 2M++ K -band luminosity function measured in Lavaux & Hudson (2011), and ROCKSTAR (Behroozi et al. 2013) halos from the DARKSKY-400 simulation (Skillman et al. 2014), a $(400 \text{ Mpc}/h)^3$ box with 4096^3 particles run with the 2HOT code (Warren 2013). Our specific abundance model will be the best-fitting one of Lehmann et al. (2015), which matches luminosity to $v_{\text{vir}}(v_{\max}/v_{\text{vir}})^{0.6}$ with a scatter of 0.16 dex. We caution that these parameters were derived using an r -band luminosity function from SDSS rather than a K -band one from 2M++, although we have verified that a basic counts-in-cells clustering statistic out to 10 Mpc is consistent between the 2M++ dataset and our abundance matched catalogue. This method enables us to generate an absolute K -band magnitude for each halo in the simulation box.¹

Next, we next calculate the absolute magnitude M of each galaxy in the 2M++ catalogue:

$$M = m - A_k(l, b) - k(z) + e(z) - D_L(z), \quad (3)$$

where m is the apparent magnitude, $A_k(l, b)$ describes dust absorption in the direction (l, b) , $k(z)$ is the k -correction due to redshifting of the spectrum, $e(z)$ is the correction for stellar population evolution, and D_L is the luminosity distance. Following Lavaux & Hudson (2011), we take $k(z) = -2.1z$, $e(z) = 0.8z$ and $A_k(l, b) = 0.35E_{(B-V)}(l, b)$, and calculate the extinction factor $E_{(B-V)}$ from the dust map of Schlegel et al. (1998). We associate each 2M++ galaxy with the halo in the simulation closest to it in absolute magnitude. We assume this halo to have an NFW profile with virial mass M_{vir} and concentration c as output by ROCKSTAR.

With this mass distribution in place, we are in position to calculate the proxy values sourced by each 2M++ object.

¹ In principle there is further information in the group statistics of the 2M++ catalogue, for two reasons. First, using the group luminosity function rather than that of individual galaxies may improve the estimate of the halo masses derived from abundance matching at the bright end. Second, the velocity dispersions of galaxies in a group provide complementary information to the luminosity on the distribution of dark matter mass. Folding this in would improve the precision of the results, although it is beyond the present scope of our work.

For Φ and \vec{a} we use standard forms for the NFW profile (Cole & Lacey 1996):

$$\Phi_{\text{vis}} = - \sum_i \frac{GM_{\text{vir},i}}{r_i} \frac{\ln(1 + \frac{c_i r_i}{R_{\text{vir},i}})}{\ln(1 + c_i) - \frac{c_i}{1+c_i}}, \quad (4)$$

$$\vec{a}_{\text{vis}} = - \sum_i \frac{GM_{\text{vir},i}}{r_i} \frac{\frac{1}{r_i} \ln(1 + \frac{c_i r_i}{R_{\text{vir},i}}) - \frac{c_i/R_{\text{vir},i}}{1+c_i r_i/R_{\text{vir},i}}}{\ln(1 + c_i) - \frac{c_i}{1+c_i}} \hat{r}_i, \quad (5)$$

for source object i at distance r_i from the test point, where \hat{r} points from the source halo centre to the test point. The subscript ‘vis’ denotes that these contributions to the proxies derive from objects visible to the 2M++ survey; further contributions will be described in Sections 2.2 and 2.3. We measure curvature using the Kretschmann scalar $K \equiv (R^{\alpha\beta\gamma\delta} R_{\alpha\beta\gamma\delta})^{1/2}$, both because it is non-zero in vacuum and to promote compatibility with Baker et al. (2015), who find it to be of use in synthesising laboratory, astrophysical and cosmological constraints on gravity. While in detail the Kretschmann scalar for a set of point masses is nonlinear, we find the error incurred by approximating it as the linear sum of individual contributions to be small. We assume also that K can be adequately calculated by treating each source halo as a point mass at its centre. As we make no attempt to estimate the accuracy of this approximation, K ought not to be considered more than an order-of-magnitude estimator of the true curvature.

$$K_{\text{vis}} = \sum_i \sqrt{48} \frac{GM_{\text{vir},i}}{r^3}. \quad (6)$$

2.2 Calibration with N-body simulations

The 2M++ catalogue does not include all mass within 200 Mpc, and hence the calculation of Section 2.1 underestimates Φ , \vec{a} and K . The contribution from unseen mass may be determined from the N-body simulation that we have already used to prescribe halo properties for the 2M++ galaxies. Our procedure for estimating this contribution is as follows:

(i) Using the absolute magnitude assigned to each halo from abundance matching, and assuming the observer to be at the centre of the box, determine the apparent magnitude from Eq. 3.² Thus split the halos into those that would be visible in the 2M++ catalogue ($m < 12.5$) and those that would not ($m > 12.5$).

(ii) At the position of each well-resolved halo (containing at least 20 particles), calculate Φ from all other halos within 10 Mpc (Φ_{hal}), and from the visible ones alone (Φ_{vis}). (It is advisable to use the positions of the halos themselves rather than random points in the box because the latter would not reproduce the clustering properties of real galaxies. In

² Although the N-body box is not intended to represent the actual local universe, we nevertheless use the angular dependence of the Schlegel et al. (1998) dust map to calculate the extinction at the position of each halo. As this term is small, a different angular dependence would have little effect.

particular, low density regions would be much more prominently represented.) Take $c_{\Phi} \equiv \Phi_{\text{hal}}/\Phi_{\text{vis}}$ as the multiplicative ‘correction factor’ required to map the visible potential onto the total one.³ Record also the distance to the halo in question (d), the number of visible objects within 10 Mpc of it (N_{10}), and Φ_{vis} . We find these observables to correlate strongly with c_{Φ} , and hence will use them to predict it.

(iii) Partition the $\{c_{\Phi}, d, N_{10}, \Phi_{\text{vis}}\}$ space into discrete cells and populate it with the halos in the box. This estimates the joint probability distribution function of these variables.

(iv) For each test galaxy in the real universe, estimate c_{Φ} by drawing a random value from this distribution function at the $\{d, N_{10}, \Phi_{\text{vis}}\}$ of that galaxy.

(v) Repeat for $c_a \equiv |\vec{a}_{\text{hal}}|/|\vec{a}_{\text{vis}}|$, $c_{\theta} \equiv \frac{\vec{a}_{\text{hal}} \cdot \vec{a}_{\text{vis}}}{|\vec{a}_{\text{hal}}||\vec{a}_{\text{vis}}|}$ and $c_K \equiv K_{\text{hal}}/K_{\text{vis}}$. (For simplicity, we will continue to use Φ_{vis} for the estimation of c_a , c_{θ} and c_K , rather than $|\vec{a}_{\text{vis}}|$ and K . We find the latter variables to correlate little better with their respective correction factors.) While c_K is directly analogous to c_{Φ} , c_a describes the change in the *magnitude* of the acceleration when unseen objects are included, while c_{θ} gives the angle through which it is rotated. To estimate the combined acceleration vector of 2M++ and unseen halo objects, we first multiply \vec{a}_{vis} by c_a , then randomly rotate the resulting vector through c_{θ} . We will collectively denote the correction factors by $\vec{c} \equiv \{c_{\Phi}, c_a, c_{\theta}, c_K\}$.

We require the correlation with observables because the N-body simulation that models the unseen mass does not represent the local universe, and hence a point-by-point comparison is not possible. However, a simulation constrained to match the 2M++ catalogue at $z = 0$ would enable the total proxy values to be determined directly at any point in space, avoiding the scatter introduced by the imperfect correlation between the correction factors and $\{d, N_{10}, \Phi_{\text{vis}}\}$. The groundwork for such a simulation has been laid by Lavaux & Jasche (2016); this approach is however beyond the present scope of our work.

2.3 Restoring the low-frequency power

There remains one further contribution to our proxies: the long-wavelength modes of the density field which are not captured by the halo model. van Daalen & Schaye (2015) find that while halos of mass $M_{200} > 10^9 h^{-1} M_{\odot}$ (corresponding roughly to the resolution limit of the DARKSKY-400 simulation) supply around 95% of the power in modes of wavelength $\lambda < 2 h^{-1} \text{Mpc}$, this fraction falls steeply at higher wavelength, reaching $\sim 30\%$ at $\lambda = 100 h^{-1} \text{Mpc}$. As long-wavelength modes will be most important in void regions with few massive nearby halos (which are least likely

³ Note that due to redshift incompleteness in the 2M++ catalogue, as discussed in Lavaux & Hudson (2011), fewer objects are actually observed than pass the magnitude cut, an effect more pronounced in some directions than others. This causes our correction factors to be underestimated, as we assume that all objects with $m < 12.5$ contribute to the observable proxies. However, as the survey achieved high completeness in all regions above the galactic disk (Lavaux & Hudson 2011), this effect is insignificant there relative to the other sources of uncertainty in our analysis.

to be screened and hence of most interest for modified gravity applications), it is imperative that we model them accurately. To do so we use the results of [Lavaux & Jasche \(2016\)](#), who calculate the $z = 0$ density field implied by the number density and peculiar velocities of the 2M++ galaxies. This analysis reconstructs density modes from $\lambda \approx 4.8 h^{-1} \text{Mpc}$ ($\delta \approx 45$) to beyond the size of the 2M++ volume, and is therefore capable of restoring all the power omitted in Sections 2.1 and 2.2. We take the density grid at a representative point in the MCMC chain of [Lavaux & Jasche \(2016\)](#),⁴ interpolate it to form a smooth density field, and then sum the contribution of this effective mass to Φ_{hal} , \vec{a}_{hal} and K_{hal} calculated above.

As some fraction of this mass is already included in Section 2.2, a simple addition overestimates the total density. However, our use of a 10 Mpc filter function for the halo contribution effectively limits it to frequencies $1/\lambda \gtrsim 0.1 \text{Mpc}^{-1}$, and hence the only region of overlap is $0.1 \text{Mpc}^{-1} \lesssim 1/\lambda \lesssim 0.14 \text{Mpc}^{-1}$ (where the upper bound is set by the $4.8 h^{-1} \text{Mpc}^{-1}$ resolution limit). We have verified by direct calculation that subtracting these modes from the [Lavaux & Jasche \(2016\)](#) density field alters our proxy estimates at no more than the percent level, and hence that they do not provide a significant source of error. The majority of the [Lavaux & Jasche \(2016\)](#) contribution comes from higher wavelength modes.

Our code for performing all the operations of this section is publicly available at www.stanford.edu/~harryd2/gravity_maps.

3 RESULTS

In a real application, our method would be used to evaluate Φ , \vec{a} and K at the positions of galaxies with measured values for potential modified gravity signals. Since we do not possess such a sample here, we instead show results at the positions of galaxies in our source catalogue, which at least sample realistic galaxy environments. In this section we will investigate the impact of unseen halo mass and the reliability of our method of estimating it (Section 3.1), the relative contributions of the three mass components (Section 3.2), and the overall proxy distributions (Section 3.3).

3.1 Modelling unseen mass

We begin with our determination of the correction factors c_Φ , c_a , c_θ and c_K : histograms of these quantities are shown in Figure 1 for galaxies within 200 and 50 Mpc. The averages and standard deviations of these distributions are reported in the second and third columns of Table 1, while the fourth contains the average dispersions at fixed values of d , N_{10} and Φ_{vis} . These measure the uncertainties on our estimate of \vec{c} using the method of Section 2.2. The most significant features of these results are the following:

⁴ The results are not significantly altered by choosing a different high-likelihood point from the chain, although see Section 4.2 for further discussion of this source of uncertainty.

(i) As the correction factors are not negligible, they are important in any calculation of Φ , \vec{a} or K . Tails towards high values indicate environments dominated by unseen mass.

(ii) On average, $c_K > c_a > c_\Phi$, and the variances of the distributions increase also in that order. This is the order of decreasing sensitivity of the proxy to the separation r of source and test point: $|\vec{a}|$ and K are more dependent than Φ on nearby low-mass objects which are less likely to be included in 2M++. This makes our method most reliable for determining Φ and least for K , as the latter is more likely to be dominated by a single faint object. Indeed, at some test points K_{hal} exceeds K_{vis} by orders of magnitude (note the logarithmic axis on Figure 1(d) and the final row of Table 1), making a method based on a magnitude-limited source galaxy sample unreliable. This is manifest in a significant variance in $\log_{10}(c_K)$ even after we have calibrated it point-by-point with $\{d, N_{10}, \Phi_{\text{vis}}\}$. K is therefore the least well measured of our proxies.

(iii) The widths of the \vec{c} distributions are significantly smaller after calibrating with $\{d, N_{10}, \Phi_{\text{vis}}\}$ than before, showing that this method improves the precision of our proxy calculations. The remaining variance contributes to the final uncertainty in our maps, as we discuss further in Section 4.2.

(iv) The correction factors are larger further away since a smaller fraction of objects passes the 2M++ magnitude cut.

3.2 Relative contributions to the proxies

Next we show in Figure 2 the relative contributions to the proxies from the observed 2M++ galaxies, the unseen matter from the N-body box, and the long-wavelength modes. That they are roughly the same order of magnitude shows that none are negligible. In the case of Φ , the 2M++ galaxies and long-wavelength modes provide roughly uniform fractional contributions, while the invisible objects in the simulation typically contribute $\sim 20\%$, and rarely more than 50%. This contribution is not dominant, indicating that a reasonable approximation to Φ can be obtained from the objects visible to current-generation galaxy surveys alone, and hence that uncertainties concerning the location of unseen mass are not huge. Some test galaxies have no or very few 2M++ source objects within 10 Mpc, making both Φ_{vis} and Φ_{hal} very small; the potential for these objects effectively derives purely from the long-wavelength modes.

Interpretation of the relative contributions of the three components to \vec{a} (Fig. 2(b)) is complicated by the fact that they do not sum directly at a given test point, but rather vectorially. Depending on the phases, this means that the magnitudes of the acceleration due to any one of the components may be larger than the total acceleration, making the fractional contribution greater than 1. The 2M++ part peaks at around 75%, and most often the remaining 25% (with roughly aligned directions) comes from unseen halos. It is also not uncommon for the 2M++ objects to contribute $\sim 95\%$ or $\sim 60\%$, and the unseen halos $\sim 5\%$ or $\sim 40\%$ respectively. Since mass in the low-frequency modes is by definition fairly homogeneous (and the zero-frequency mode entirely so), it tends to have little effect on the acceleration as contributions from opposite sides of the test galaxy roughly cancel out. That said, the small fraction of test points with little 2M++ or unseen halo mass within

Correction factor	Median	Mean	St. dev.	St. dev. after calibration
c_Φ	1.5	2.1	2.7	0.19
c_a	1.2	5.8	65.0	2.1
c_θ	0.17	0.45	0.61	0.42
$\log_{10}(c_K)$	0.7	1.1	1.2	0.70

Table 1. Statistics describing the distributions of correction factors relating proxy values from 2M++ objects to those from all halo mass. ‘‘Calibration’’ refers to our procedure for estimating the correction factors from $\{d, N_{10}, \Phi_{\text{vis}}\}$ (Section 2.2), which can be seen to reduce their uncertainties.

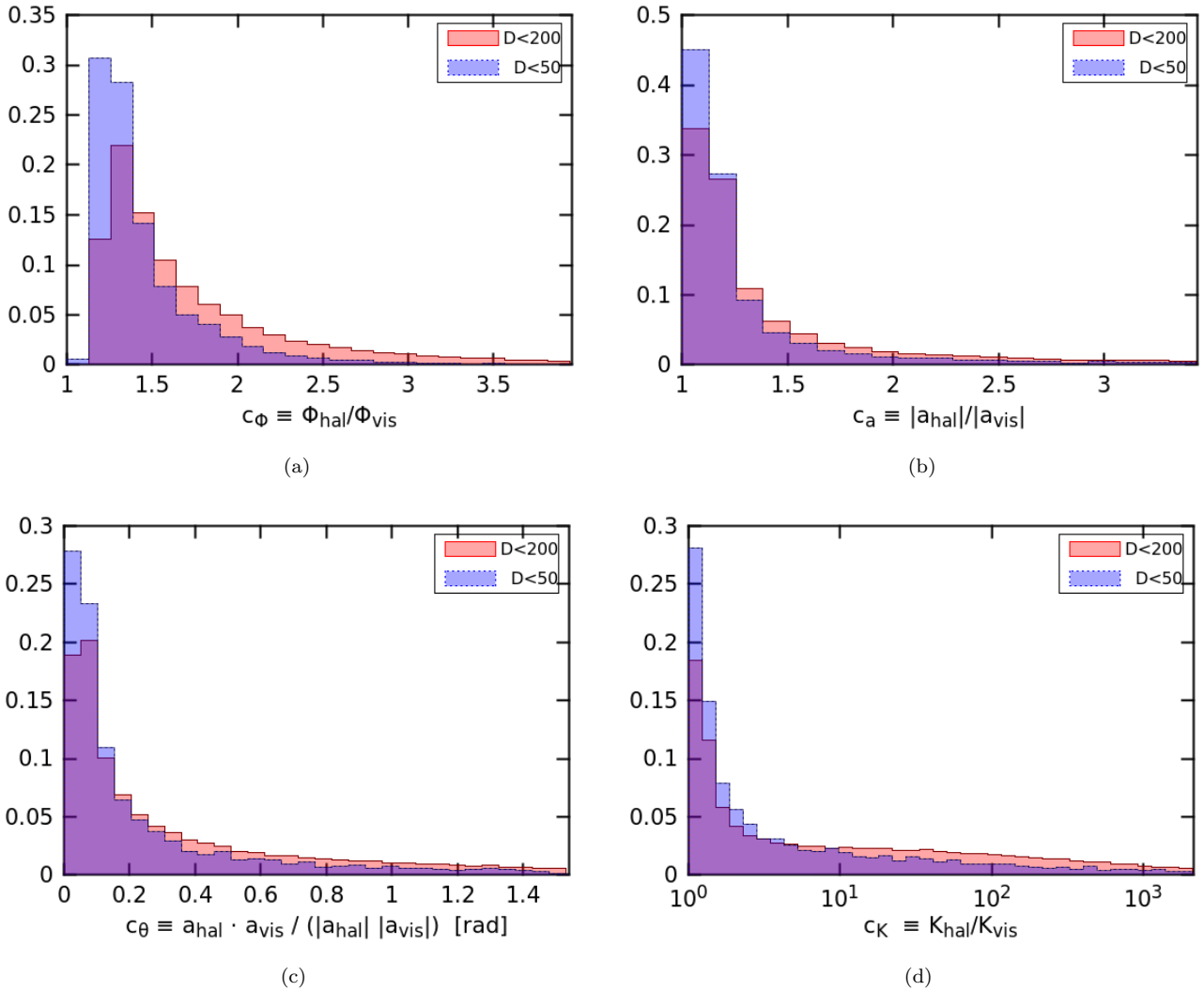


Figure 1. The distributions of the correction factors relating the contributions to Φ (c_Φ , Fig. 1(a)), \vec{a} (c_a , Fig. 1(b)) and c_θ , Fig. 1(c)) and K (c_K , Fig. 1(d)) from 2M++ objects (subscript ‘vis’) to those from all halos (‘hal’). c_a describes the change in magnitude of the acceleration vector, and c_θ the angle through which it is rotated (see Section 2.2). The correction factors typically increase with distance from the observer.

10 Mpc have accelerations dominated by the low-frequency modes, as evidenced by the peak in the green curve at ~ 1 .

In the case of curvature (Fig. 2(c)), we find K typically to be dominated by a single component, most often the unseen halos. As mentioned in Section 3.1, this is because K falls steeply with r and is therefore strongly affected

by nearby low-mass objects. Since K samples on average a much smaller volume around a given test galaxy than Φ or \vec{a} , it is less affected by mass in long-wavelength modes, rendering this contribution largely negligible.

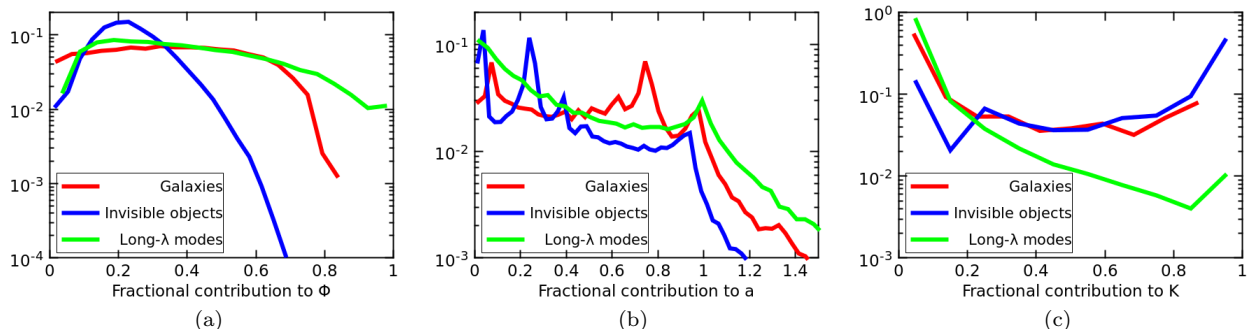


Figure 2. The relative contributions to Φ , \vec{a} and K of the 2M++ galaxies, unseen halo mass and long-wavelength density modes. Since contributions to \vec{a} sum vectorially, the magnitude of the acceleration from a given component may be larger than that of the total.

3.3 Distributions of gravitational variables

Figure 3 shows the distributions of Φ , \vec{a} and K across our test objects, including source objects up to $r_{\max} = 10$ Mpc (red) or 3 Mpc (blue). As mentioned in Section 1, the choice of r_{\max} is important for Φ due to its weak fall off with the separation of test and source object. It is also somewhat important for K : for small r_{\max} , some test points receive very little contribution from either the 2M++ galaxies or unseen halo mass and hence have K values set by the near-irreducible background from the long-wavelength modes ($K \approx 10^{-56} \text{ cm}^{-2}$, corresponding roughly to the “Lambda” line in fig. 1 of Baker et al. 2015). For \vec{a} , objects more distant than 3 Mpc contribute little and the long-wavelength background is largely unimportant. We find the proxy distributions not to depend significantly on the masses of the test galaxies, and thus they provide an indication of the range of values probed by any galaxy sample without explicit selection on environment.

Finally, in Figure 4 we display the proxy values across a 300 Mpc \times 300 Mpc slice of the local universe with a sampling resolution of 1.5 Mpc. The increasingly detailed level of structure in these maps when moving from Φ to a to K reflects the greater sensitivity of the proxy to the separation r of source and test points. Note also that Fig. 4(c) likely manifests the larger uncertainty (mentioned in Section 3.1) in our calculation of K than Φ or a . While Figs. 4(a) and 4(b) are roughly uniform over the entire area, as expected, Fig. 4(c) has two rare features close to the observer. This likely indicates that similar features further away are poorly reconstructed by our method for incorporating mass below the magnitude limit of the 2M++ survey.

These maps reveal promising regions for modified gravity applications; for example, regions of deep blue in Fig. 4(a) have very low Φ/c^2 (down to few $\times 10^{-7}$), allowing any galaxies within them to remain unscreened in chameleon theories with small background scalar field values. Conversely, regions of deep red in Fig. 4(b) have particularly high accelerations, making them most likely to harbour external field-dominated galaxies in MOND.

4 DISCUSSION

In this section we discuss the implications of our results for galaxy-scale tests of modified gravity (Section 4.1), and

then describe the major uncertainties in our maps and the potential for future improvement (Section 4.2).

4.1 Applications to modified gravity

We begin with a few general inferences about the usefulness of galaxy-scale tests of gravity from the distributions of our proxy values (Fig. 3).

(i) In chameleon scalar-tensor theories, the value of Φ marking the transition between the screened and unscreened regimes is set by the background value of the scalar field (Hu & Sawicki 2007). A test of screening involves a comparison between putatively screened and unscreened samples, and hence the lowest value of Φ determines the strength of the constraint that may in principle be placed on the theory. Figure 3(a) shows that while a large fraction of galaxies have $\Phi/c^2 \lesssim 10^{-5}$ for $r_{\max} = \lambda_C = 10$ Mpc (see Eqs. 1 and 2), very few have $\Phi/c^2 \lesssim 10^{-6}$ for $r_{\max} = \lambda_C = 3$ Mpc. This suggests that it is unlikely for galaxy-scale tests to be capable of probing f_{R0} to much below 10^{-6} .

This conclusion is somewhat more pessimistic than that of Cabré et al. (2012), who claim that dwarf galaxies have the potential to probe field values down to $f_{R0} \sim 10^{-8} - 10^{-7}$. This discrepancy is due to two main factors. First, by assuming that all the galaxy mass in a group is located at the group’s centre, Cabré et al. (2012) underestimate the group’s contribution to Φ at distances beyond around a third of its virial radius (relative to Eq. 4). In our calculation the source mass is more homogeneously distributed, due both to the retention of individual galaxies’ masses within groups, and to our use of NFW halo profiles. We estimate that this typically affects Φ by a factor ~ 3 . Second, Cabré et al. (2012) neglect the contribution to Φ from low-mass halos hosting galaxies too faint to be measured in current galaxy surveys, and from the mass in linear and quasi-linear modes of the density field. We see from Fig. 1(a) and the first row of Table 1 that the former typically boosts the potential by a factor 1.1–3, while the latter introduces a near-irreducible background of $\Phi \sim \text{few} \times 10^{-7}$. Even in void regions with few or no nearby halos, this background would be sufficient to initiate screening for f_{R0} much below this value.⁵

⁵ In the context of scalar-tensor theories the ultimate measure of a proxy is the precision with which it estimates the true degree

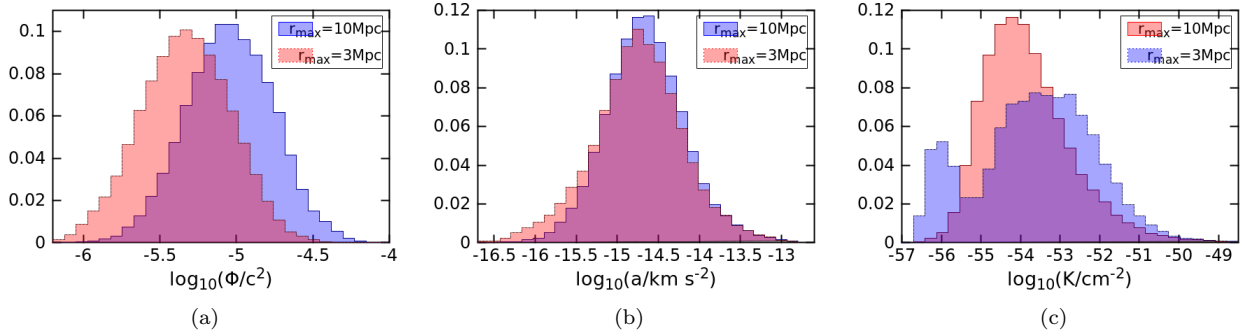


Figure 3. Distributions of Φ , \vec{a} and K at the locations of the 2M++ galaxies, calculated within a sphere of 10 Mpc (blue) or 3 Mpc (red) around each test point. The ranges of these variables set the potential of galaxies to extend the scope of probes of modified gravity.

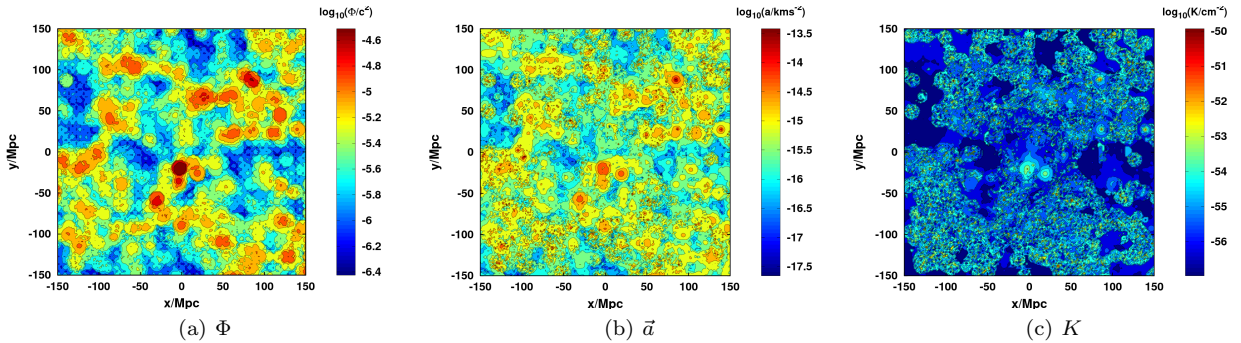


Figure 4. Contour plots of Φ , \vec{a} and K across a 300 Mpc \times 300 Mpc slice of the local universe. The Milky Way is located at $x = y = 0$.

(ii) Typical external accelerations are approximately a few $\times 10^{-15}$ km s $^{-2}$, with a range of $\sim 10^{-16} - \text{few} \times 10^{-14}$ (Fig. 3(b)). This is largely independent of the distance $r_{\text{max}} \gtrsim 3$ Mpc out to which source objects are considered. In MOND-type models, a galaxy enters the external field-dominated regime when the external acceleration a_{ex} , due to surrounding mass, exceeds the acceleration a_{in} generated by the galaxy itself, provided a_{in} is less than the characteristic acceleration $a_0 \approx 1.2 \times 10^{-13}$ km s $^{-2}$. Thus our distribution of a_{ex} indicates the maximum internal accelerations – and hence surface densities – that galaxies can have for the external field to be important. A typical value $a_{\text{ex}} \sim \text{few} \times 10^{-15}$ km s $^{-2}$ would correspond to surface density $\Sigma \approx 20 M_{\odot} \text{pc}^{-2}$, which is very small even for a low surface brightness galaxy. Thus only unusually high a_{ex} values would appreciably impact dynamics. Galaxies with $a_{\text{ex}} > a_0$ (of which Fig. 3(b) suggests there are very few) should exhibit fully Newtonian behaviour. We caution however that we have measured the proxies only at the positions of the 2M++ galaxies; more promising galaxies for tests of the external field effect are dwarfs very close to a single massive object which provides the bulk of the external acceleration (such as the dSphs of the Milky Way and M31; [McGaugh &](#)

[Milgrom 2013a,b](#)). It is unlikely that these would be included among our test galaxies due to high apparent magnitudes at any distance beyond the local group. At the positions of such galaxies located by other means, however, our map would be expected to report a_{ex} accurately provided the galaxies sourcing the field were included in the 2M++ catalogue.

At the other end of the scale, by spherical symmetry (and unlike for Φ and K), low-frequency density modes do not provide an irreducible background value of \vec{a} , and hence there is no fundamental reason why regions of arbitrarily low \vec{a} could not exist. This enables screening mechanisms characterised by acceleration (e.g. kinetic) to be tested in principle to arbitrary precision in galaxies, provided a sample in sufficiently remote environments could be compiled.

(iii) The external curvature is typically around $K = 10^{-54}$ cm $^{-2}$, with a range of roughly $10^{-56} - 10^{-50}$. This sets the precision with which Vainshtein screening may be tested at the galaxy scale. These values are at the low end of the “curvature desert” identified in [Baker et al. \(2015\)](#), enabling galaxies potentially to inhabit any part of this region when their internal curvature contributions are added.⁶ As K falls off rapidly with r , these contributions will typically greatly exceed the environmental ones considered here.

More detailed or model-specific conclusions concerning

of screening, and it is possible that a quantity assuming point masses is better in this regard than one derived from more realistic mass profiles. However, our method likely better estimates the Newtonian potential, and hence is better suited both to comparison with [Baker et al. \(2015\)](#) and to the calculation of more physical quantities such as acceleration.

⁶ [Baker et al. \(2015\)](#) consider only the internal contributions. For models in which the important variable is the total proxy value, our results should therefore be considered summed to the galaxy lines in [Baker et al. \(2015\)](#)’s fig. 1.

modified gravity will require a test galaxy sample for which measurements of potential modified gravity signals have independently been made. Correlations of these signals with the proxies determined from our maps (plus the internal contributions from the galaxies themselves) may then be used to search for a transition to a new gravitational regime or test specific theories for which these proxies are important.

Such signals will depend on the theory in question. In scalar-tensor theories, the stars in unscreened galaxies may self-screen, leading to differences in their kinematics with those of the gas and dark matter. In particular, the stars would fall more slowly in an external field, leading to displacements between the centroids of stellar and HI disks preferentially aligned with the external acceleration, and to a difference between H α and HI rotation curves. The offset between halo and disk centres may then cause stellar disks to warp (Jain & VanderPlas 2011; Vikram et al. 2013).

In MOND, the value of $|\vec{a}|$ sets the ratio of a system's dynamical to baryonic mass, and also the shape of the rotation or velocity dispersion profile. In galaxies with internal acceleration $a_{\text{in}} \ll a_0$, rotation curves would be flat for $a_{\text{ex}} < a_{\text{in}}$ (the standard deep-MOND regime), but Keplerian for $a_{\text{ex}} > a_{\text{in}}$ (the external field-dominated regime; Famaey & McGaugh 2012). The galaxy's total mass discrepancy, measured by $\mathcal{D} \equiv \frac{RV^2}{M_{\text{bar}}G}$, would then be $\sim a_0/a_{\text{ex}}$ for $a_{\text{ex}} < a_0$ (the quasi-Newtonian regime) and 1 for $a_{\text{ex}} > a_0$ (the Newtonian limit). The correlation of \mathcal{D} with a_{ex} – the external-field analogue of the mass discrepancy–acceleration relation (McGaugh 1999; Lelli et al. 2017) – would have a characteristic shape and a feature at $a_{\text{ex}} = a_0$.

Finally, we note that our maps may also find application in the study of galaxy formation. While correlations between Φ , a or K and galaxy signals may be evidence for novel gravitational physics, they would more likely attest to galaxy growth or evolution effects in Λ CDM. They may therefore be useful in studies of quenching, conformity, satellite–host interactions and the environment dependence of the galaxy–halo connection. These phenomena will constitute important systematics in tests of gravity.

4.2 Error analysis & future prospects

Here we describe the most significant sources of uncertainty in our maps. This will give an indication of the areas on which future analyses should focus to best improve precision, and the ways in which upcoming galaxy surveys will be able to contribute.

(i) Galaxies of given luminosity may reside in halos with a range of masses and concentrations, so that the observed distribution of light does not uniquely determine the distribution of total mass. Thus the 2M++ galaxy sample corresponds to a range of possible Φ_{vis} , \vec{a}_{vis} and K_{vis} fields, of which the ones we show are simply example realisations. The tighter the galaxy–halo connection (as quantified in our framework by the abundance matching scatter), the smaller this source of uncertainty.

(ii) We estimated the correction factors required to convert the proxies sourced by visible mass to their true, total values on a point-by-point basis using their correlations with distance, the number of 2M++ objects within 10 Mpc, and the potential from these objects. However, as shown in

Table 1, significant uncertainties remain, especially for $|\vec{a}|$ ($\sim 200\%$) and K (~ 0.7 dex). These factors increase with distance. Since this uncertainty derives from the fraction of objects included in the galaxy survey, it is best reduced by employing a deeper survey. Over a third of the sky the magnitude limit may already be improved by using the SDSS main sample, with a Petrosian r -band magnitude limit of 17.7, and the Taipan survey will soon provide similar data in the South. Within the next decade, the Dark Energy Spectroscopic Instrument (DESI) will push around two magnitudes deeper, directly locating an even greater proportion of the local universe's mass. This will significantly reduce the fraction of mass that must be inferred from N-body simulations, and hence the corresponding uncertainties in the proxies. To quantify this we show forecasts for a DESI-like galaxy catalogue in Table 2, assuming a limiting r -band magnitude of 19.7 and average $r - K$ colour of 2.7 (e.g. Bell et al. 2003). The uncertainties on the correction factors are reduced by a factor of several. (DESI will also provide significantly enhanced spectroscopic information, which may be used to improve our proxy estimates.) We refer the reader to Jain (2011), Jain & Khoury (2010) and Jain et al. (2013) for further discussion of survey requirements and optimisation for the purposes of gravitational physics.

Alternatively, as mentioned in Section 2.2, an N-body simulation constrained to reproduce a galaxy survey such as 2M++ may be used to estimate the location of unseen mass relative to the observed light. Although it is unlikely that this method would locate low-mass substructure accurately, it would reduce the correction factors due to invisible mass and hence increase the precision of the maps. Another way to reduce the correction factors would be to supplement the catalogue with galaxies from other sources, such as NED. This would come at the cost of rendering the observational selection criteria inhomogeneous, making it harder to determine which objects in the N-body simulation would be included and which not.

(iii) The properties of the halos associated with each source galaxy receive uncertainties from the following: 1) Uncertainties in the abundance matching parameters used to link galaxy magnitude to halo mass and concentration. The values we adopt were shown by Lehmann et al. (2015) to reproduce r -band clustering statistics in SDSS, but there is no guarantee that they will match in detail the K -band clustering of 2M++. 2) The internal structures of halos are modified by baryonic physics through a combination of adiabatic contraction of dark matter and feedback processes (e.g. Blumenthal et al. 1986; Governato et al. 2010; Pontzen & Governato 2012), which will affect the proxy values close to halos. 3) Resolution effects may make the masses, concentrations and positions of small halos unreliable. In particular, it is known that N-body simulations overpredict in general the amount of low-mass substructure in the universe (Klypin et al. 1999; Boylan-Kolchin et al. 2011), potentially causing the correction factors to be overestimated.

(iv) The analysis of Lavaux & Jasche (2016) derives a posterior probability distribution for the quasi-linear density field of the local universe from the positions and velocities of the 2M++ galaxies. The uncertainty that the width of this distribution propagates into our maps may be estimated by averaging over the results from all field configurations in the posterior, effectively marginalising over the possibilities. By

Correction factor	Mean	St. dev.
c_Φ	1.3	0.43
c_a	1.8	12.3
c_θ	0.22	0.42
$\log_{10}(c_K)$	0.46	0.74

Table 2. As Table 1 (middle two columns), but for a DESI-like galaxy catalogue with limiting magnitude $m_r = 19.7$. A far greater fraction of the mass sourcing the proxies will be directly visible to the survey.

direct substitution of several high-likelihood configurations, however, we have verified that the resulting uncertainty in our final proxy estimates is subdominant to the effects described above, and hence we do not pursue it further here.

(v) Uncertainties in the measured magnitude, position and distance of each source object propagate into uncertainties in our maps.

These sources of uncertainty may all be accounted for in tandem by generating many realisations of the proxy maps with each input parameter drawn randomly from the allowed set of values. We leave this full error propagation for future work, but caution that it may be critical for determining the significance level with which a given set of galaxies falls into a certain gravitational regime.

A full comparison with modified gravity expectations would have further uncertainties. To make predictions for a specific theory, it would likely be invalid in detail to assume Λ CDM to calculate the halo mass function, the galaxy–halo connection, the relation between absolute and apparent magnitude, or the quasi-linear modes of the 2M++ field. We justify our doing so by arguing that the types of modified gravity theory that motivate our work are likely to generate larger deviations from GR on galactic than cosmological scales. The impact on cosmology – and hence those parts of our analysis that rely on Λ CDM – would be a second order effect in the prediction of the final signals.

This argument is *a priori* least plausible in the case of MOND, which is unique among the models motivating our work in that it seeks to eliminate dark matter. MOND is not connected continuously to GR and Λ CDM as scalar-tensor theories are, but rather postulates a discrete deviation at the level of the Newtonian limit. The level of systematic error between our calculated \vec{a} and that in MOND likely depends on the specific formulation of the theory. In QUMOND (Milgrom 2010), the MOND acceleration is simply an algebraic function of the Newtonian acceleration due to baryons alone, and the difference may therefore be represented by a distribution of “phantom dark matter.” Although there is no *a priori* reason why this distribution should be correctly given by abundance matching (for one there is no longer a halo mass function), the fact that observational estimates of the relation between visible and dynamical mass roughly agree with the abundance matching prediction (Behroozi et al. 2010) suggests that this technique would give a sensible estimate for the amount of phantom dark matter as a function of luminosity in the mass range of interest. We would however expect c_a to be nearer 1 in this case, as there would

be no contribution to \vec{a} from mass unassociated with light. As this tends to increase $|\vec{a}|$, our result would constitute an upper limit on the external acceleration field in MOND, making our conclusion that there are very few objects in the fully external field-dominated regime robust.

Other formulations, however, include a curl field in the relation between Newtonian and MONDian acceleration, which introduces further nonlinearities into the dependence of the total acceleration on the (baryonic) mass distribution, in addition to a potential offset between the direction of the true acceleration and the one we have calculated (e.g. Llinares et al. 2008; Famaey & McGaugh 2012). In such cases our method may give a poor approximation to the acceleration governing the MOND external field effect; we leave further investigation of this effect to future work.

Ultimately, random uncertainties in the proxies will tend to blur any correlation with potential modified gravity signals, while systematic uncertainties may introduce spurious correlations. The magnitude of the total uncertainty therefore sets the minimum signal strength that would be statistically significant.

5 CONCLUSION

We have combined an all-sky galaxy catalogue, a high-resolution N-body box and an estimate of the linear and quasi-linear density modes of the local universe to map the gravitational potential Φ , acceleration \vec{a} and curvature K to a distance of 200 Mpc. As the fundamental variables of the gravitational field, these may be expected on general grounds to mark the transitions between gravitational regimes, and at the galaxy scale they are of specific importance in screened scalar-tensor theories and EP-violating models such as MOND. We use our maps to determine the sensitivity that galaxy-scale tests of modified gravity may be expected to achieve, and identify promising regions of the local universe. Our method may be easily adapted to any source and test galaxy sample, and we make public the code for doing so.

From the overall distributions of the gravitational variables we draw four general conclusions.

- When calculated in spheres of radius 3–10 Mpc (typical Compton wavelengths of a light scalar field), the distribution of Φ/c^2 peaks at around a few $\times 10^{-6} - 10^{-5}$, and has a minimum of a few $\times 10^{-7}$ set by the long-wavelength modes of the density field. Since the background scalar field in chameleon-screened scalar-tensor theories (e.g. f_{R0} in $f(R)$ gravity) is of order the threshold in Φ/c^2 at which screening becomes operative, it is unlikely that astrophysical measurements are capable of constraining this to much below $\sim 10^{-6}$. This conclusion holds no matter how weak a galaxy’s own internal contribution to Φ , and suggests that galaxy-scale tests may ultimately prove less constraining than those based on cepheids and other local distance indicators (Jain et al. 2013). They are however significantly stronger than cosmological probes (e.g. Lombriser et al. 2012).

- The external acceleration field is typically around a few $\times 10^{-15} \text{ km s}^{-2}$ and rarely exceeds the characteristic acceleration $a_0 \approx 10^{-13} \text{ km s}^{-2}$ at which visible and dynamical masses diverge. Thus, in the context of MOND-type models, few objects will generically be in the fully external field-

dominated regime in which dynamics is Newtonian even for arbitrarily small internal acceleration. Locating such objects to test the external field effect would therefore require targeted searches around known mass concentrations.

- Curvature values are centred around 10^{-54} cm^{-2} , at the low end of the “curvature desert” that Baker et al. (2015) identifies as a potentially interesting region for modified gravity.

- The precision with which Φ , \vec{a} and K may be mapped is limited by our ability to detect faint objects at large distance. Galaxy catalogues from future surveys such as DESI and LSST will therefore greatly reduce uncertainties: we estimate that with a magnitude limit of $m_K \approx 17$, achievable by DESI, the fraction of Φ for typical galaxies that will be unaccounted for by measured mass alone will be only $\sim 30\%$.

ACKNOWLEDGEMENTS

We thank Julien Devriendt, Bhuvnesh Jain, Vinu Vikram and Risa Wechsler for helpful discussions during the course of this work, and Tessa Baker, Gary Mamon and Stacy McGaugh for comments on the manuscript. HD received support from the Balzan foundation via New College, Oxford, and from the U.S. Department of Energy under contract number DE-AC02-76SF00515. PGF is supported by ERC H2020 693024 GravityLS project, the Beecroft Trust and STFC. GL acknowledges financial support from “Programme National de Cosmologie and Galaxies” (PNCG) of CNRS/INSU, France. GL is supported by ANR grant ANR-16-CE23-0002.

This work made use of the Dark Sky simulations, which were produced using an INCITE 2014 allocation on the Oak Ridge Leadership Computing Facility at Oak Ridge National Laboratory. We thank the Dark Sky collaboration for creating and providing access to this simulation, and Sam Skillman and Yao-Yuan Mao for running ROCKSTAR and CONSISTENT TREES on it, respectively. Additional computation was performed at SLAC National Accelerator Laboratory.

This research was supported by the DFG cluster of excellence “Origin and Structure of the Universe” (www.universe-cluster.de). This work was partly made in the ILP LABEX (under reference ANR-10-LABX-63) supported by French state funds managed by the ANR within the Investissements d’Avenir programme under reference ANR-11-IDEX-0004-02.

REFERENCES

Babichev E., Deffayet C., Ziour R., 2009, *International Journal of Modern Physics D*, 18, 2147
 Baker T., Ferreira P. G., Skordis C., 2013, *PRD*, 87, 024015
 Baker T., Psaltis D., Skordis C., 2015, *ApJ*, 802, 63
 Behroozi P. S., Conroy C., Wechsler R. H., 2010, *ApJ*, 717, 379
 Behroozi P. S., Wechsler R. H., Wu H.-Y., 2013, *ApJ*, 762, 109
 Bell E. F., McIntosh D. H., Katz N., Weinberg M. D., 2003, *ApJS*, 149, 289
 Blumenthal G. R., Faber S. M., Flores R., Primack J. R., 1986, *ApJ*, 301, 27
 Boylan-Kolchin M., Bullock J. S., Kaplinghat M., 2011, *MNRAS*, 415, L40
 Bull P. et al., 2016, *Physics of the Dark Universe*, 12, 56

Cabr e A., Vikram V., Zhao G.-B., Jain B., Koyama K., 2012, *JCAP*, 7, 034
 Clifton T., Ferreira P. G., Padilla A., Skordis C., 2012, *PhysRep*, 513, 1
 Cole S., Lacey C., 1996, *MNRAS*, 281, 716
 Conroy C., Wechsler R. H., Kravtsov A. V., 2006, *ApJ*, 647, 201
 Desmond H., 2017, *MNRAS*, 464, 4160
 Desmond H., Wechsler R. H., 2015, *MNRAS*, 454, 322
 Desmond H., Wechsler R. H., 2017, *MNRAS*, 465, 820
 Famaey B., McGaugh S. S., 2012, *Living Rev. Relativ.*, 15, 10
 Governato F. et al., 2010, *Nature*, 463, 203
 Hu W., Sawicki I., 2007, *PRD*, 76, 064004
 Hui L., Nicolis A., Stubbs C. W., 2009, *PRD*, 80, 104002
 Jain B., 2011, *Philosophical Transactions of the Royal Society of London Series A*, 369, 5081
 Jain B., Khoury J., 2010, *Annals of Physics*, 325, 1479
 Jain B., VanderPlas J., 2011, *JCAP*, 10, 032
 Jain B., Vikram V., Sakstein J., 2013, *ApJ*, 779, 39
 Jain B. et al., 2013, preprint (arXiv:1309.5389)
 Khoury J., Weltman A., 2004, *PRD*, 69, 044026
 Khoury J., 2013, preprint (arXiv:1312.2006)
 Klypin A., Kravtsov A. V., Valenzuela O., Prada F., 1999, *ApJ*, 522, 82
 Kravtsov A. V., Berlind A. A., Wechsler R. H., Klypin A. A., Gottlober S., Allgood B., Primack J. R., 2004, *ApJ*, 609, 35
 Lavaux G., Hudson M. J., 2011, *MNRAS*, 416, 2840
 Lavaux G., Jasche J., 2016, *MNRAS*, 455, 3169
 Lehmann B. V., Mao Y.-Y., Becker M. R., Skillman S. W., Wechsler R. H., 2015, preprint (arXiv:1510.05651)
 Lelli F., McGaugh S. S., Schombert J. M., Pawlowski M. S., 2017, *ApJ*, 836, 152
 Llinares C., Knebe A., Zhao H., 2008, *MNRAS*, 391, 1778
 Lombriser L., Slosar A., Seljak U., Hu W., 2012, *PRD*, 85, 124038
 McGaugh S. S., 1999, *Galaxy Dynamics – A Rutgers Symposium*, *Astron. Soc. Pacific Conf. Ser.*, ed. D.R. Merritt, M. Valluri, J.A. Sellwood, Vol. 182 (San Francisco: ASP), p. 528
 McGaugh S., Milgrom M., 2013, *ApJ*, 766, 22
 McGaugh S., Milgrom M., 2013, *ApJ*, 775, 139
 Milgrom M., 1983, *ApJ*, 270, 365
 Milgrom M., 1983, *ApJ*, 270, 371
 Milgrom M., 1983, *ApJ*, 270, 384
 Milgrom M., 2010, *MNRAS*, 403, 886
 Moster B. P., Somerville R. S., Maulbetsch C., van den Bosch F. C., Macci o A. V., Naab T., Oser L., 2010, *ApJ*, 710, 903
 Nordtvedt K., 1968, *Physical Review*, 169, 1017
 Pontzen A., Governato F., 2012, *MNRAS*, 421, 3464
 Reddick R. M., Wechsler R. H., Tinker J. L., Behroozi P. S., 2013, *ApJ*, 771, 30
 Schlamminger S., Choi K.-Y., Wagner T. A., Gundlach J. H., Adelberger E. G., 2008, *PRL*, 100, 041101
 Schlegel D. J., Finkbeiner D. P., Davis M., 1998, *ApJ*, 500, 525
 Skillman S. W., Warren M. S., Turk M. J., Wechsler R. H., Holz D. E., Sutter P. M., 2014, preprint (arXiv:1407.2600)
 Trujillo-Gomez S., Klypin A., Primack J., Romanowsky A. J., 2011, *ApJ*, 742, 16
 Vainshtein A. I., 1972, *Phys. Lett. B*, 39, 393
 van Daalen M. P., Schaye J., 2015, *MNRAS*, 452, 2247
 Vikram V., Cabr e A., Jain B., VanderPlas J. T., 2013, *JCAP*, 8, 020
 Wang J., Hui L., Khoury J., 2012, *PRL*, 109, 241301
 Warren M. S., 2013, *Proc. Int. Conf. High Perform. Comput. Netw. Storage Anal.*, (New York: ACM), p. 72
 Will C. M., 1993, *Theory and Experiment in Gravitational Physics*, Cambridge, CUP, 1993

This paper has been typeset from a $\text{\TeX}/\text{\LaTeX}$ file prepared by the author.